Nonorthogonal Interleave-Grid Multiple Access Scheme for Industrial Internet of Things in 5G Network

Su Hu, Bin Yu, Chen Qian, Yue Xiao, Qi Xiong, Chengjun Sun, and Yuan Gao, *Member, IEEE*

***Abstract*—To supporting the systematic requirements of higher spectrum efficiency and user deployment density in future Industrial Internet of Things (IIoT), traditional orthogonal multiple access schemes, such as orthogonal frequency-division multiplex, are quite limiting. Nonorthogonal multiple access (NoMA) has been recognized as one of the enabling technologies for IIoT in 5G network. In this paper, we have proposed an alternative NoMA scheme called interleave-grid multiple access (IGMA). Depending on interleaving and grid-mapping process, IGMA is capable to provide reliable block error rate performance, marvelous user multiplexing capability, as well as robustness against intercell interference. IGMA can apply various detection and decoding techniques at receiver sides to improve the detection performance with acceptable complexity. Both of link-level and system-level results show the promising benefits of IGMA, in particular that nearly seven times user multiplexing gain compared with orthogonal frequency-division multiple access has been observed in the system-level simulation. In addition, a hardware test bed has been implemented to verify the IGMA performance and the testing results proved the strong competitiveness of IGMA over orthogonal frequency-division multiple access in terms of block error rate performance in user overloading scenarios.**

***Index Terms*—5G, Industrial Internet of Things (IIoT), interleave, nonorthogonal multiple access (NoMA), user overloading.**

Manuscript received June 3, 2018; accepted July 9, 2018. Date of publication July 20, 2018; date of current version December 3, 2018. This work was supported in part by the Beijing Samsung Telecom R&D Center, in part by the MOST Program of International S&T Cooperation under Grant 2016YFE0123200, and in part by the National Natural Science Foundation of China under Grant 61471100/61701503. Paper no. TII-18-1429. *(Corresponding author: Su Hu.)*

S. Hu and Y. Xiao are with the National Key Laboratory on Communications, University of Electronic Science and Technology of China, Chengdu 611731, China (e-mail: husu@uestc.edu.cn; xiaoyue@uestc.edu.cn).

B. Yu, C. Qian, Q. Xiong, and C. Sun are with the Beijing Samsung Telecom Research and Development Center, Beijing 100000, China (e-mail: bin82.yu@samsung.com; chen.qian@samsung.com; q1005.xiong@samsung.com; chengjun.sun@samsung.com).

Y. Gao is with the Department of Electronic Engineering, Tsinghua University, Beijing 100084, China, and also with the Academy of Military Science of the People's Liberation Army, Beijing 100091, China (e-mail: yuangao08@tsinghua.edu.cn).

Color versions of one or more of the figures in this paper are available online at http://ieeexplore.ieee.org.

Digital Object Identifier 10.1109/TII.2018.2858142

I. Introduction

TO SUPPORT different demands of various scenarios that should be realized by 5G wireless communication systems, especially in the context of Industrial Internet of Things (IIoT) [1], a number of new technologies have been proposed. Typically, nonorthogonal multiple access (NoMA) is one of the promising candidates for significantly increasing the number of connections in IIoT [2], [3]. The utilization of NoMA in IIoT can be described as the following aspects. For massive machine-type communications (mMTC) services in IIoT scenarios, the sensor connection density shall reach 10^6 devices/km^2, whereas the spectrum efficiency shall be further improved for enhanced mobile broadband service (eMBB). Finally, the demand of reducing the transmission latency while keeping the communication reliability is the key target for ultrareliable and low latency communications (URLLC) in IIoT scenarios [4]. Thus, how to contribute all three cases is making the development of NoMA schemes absolutely appealing.

In the current literature, the research works of NoMA have been widely developed toward enhanced spectrum efficiency compared to traditional orthogonal multiple access. More specifically, in [5], Viterbi proved that nonorthogonal transmission could achieve better transmission performance by utilizing all the bandwidth for coding. Following the idea of [5], a series of research works toward nonorthogonal transmission have been proposed as in [6]–[14]. Especially, in [13] and [14], Ping *et al.* proposed a class of efficient NoMA techniques as interleave division multiple access (IDMA), which utilizes the chip-level interleaver for distinguishing multiple users. Recently, with the boost of mMTC, lots of new NoMA techniques have been proposed as in [15]–[19]. These aforementioned NoMA techniques could achieve different balanced tradeoff among spectrum efficiency, number of maximum connections, transmission performance, and invoked complexity for NoMA detector.

In general, a NoMA scheme contains the sophisticatedly designed signal processing part (e.g., interleaving, spreading, and/or sparse mapping) at transmit side and corresponding deprocessing part to handle multiuser interference (MUI) at receiver side. NoMA, allowing for sharing the same time–frequency resource among multiple users concurrently, targets to support adaptability toward massive connections, higher spectrum efficiency with greater flexibility, as well as strong robustness against channel variance and MUI, for fitting emerging

application scenarios. In conjunction with the design of grant-free transmission, the NoMA scheme should further achieve less latency, less signaling overhead, importantly without the reduction of desired communication reliability.

Driven by supporting new verticals and improving better user experience for variant new services, RAN plenary #75 is targeting for concluding the potentials of NoMA for 5G application scenarios, including IIoT [4]. This study will progress on the evaluation of NoMA schemes focusing on uplink, and provide recommendation on the NoMA scheme(s) to be specified later on. The detailed transmit-side design including bit-level and/or symbol-level processing will be discussed along with the related procedure design, e.g., hybrid automatic repeat request (HARQ) process, link adaption, etc. Generally speaking, this nonorthogonal characteristic is pronouncedly attractive when system load increases via using overlapped resource. The benefits of NoMA, particularly when enabling grant-free transmission, may encompass a variety of use cases or deployment scenarios, including eMBB, URLLC, mMTC, etc.

Followed by the concept of low density spreading introduced in [16], sparse code multiple access (SCMA) [16] and pattern division multiple access [17] have been proposed. Meanwhile, multiuser shared access, which is based on sequence design approaches, has been proposed by utilizing the specially designed low correlated spreading sequences [18]. For detection of multiple users, the successive interference cancelation is adopted for suppressing MUI. However, the spreading process is not always favorable especially in terms of performance for those NoMA schemes. The study in [19] shows that the performance can be improved by replacing spreading with low coding rate. Moreover, the number of supported users for schemes like SCMA, etc., is still limited by the specially designed spreading sequence. When enjoying merits from the sparsity, practical systems are also concerning the implementation complexity at the receiver side. Meanwhile, when using the elementary signal estimator (ESE), this simple detector still requires the low coding rate to guarantee the detection performance, and the detection performance degrades in high coding rate. The detection complexity by using near-optimal algorithms like MPA or MAP will be considerably high. Therefore, achieving the balance/flexibility on complexity control and performance obtaining is vital to design a practical NoMA scheme.

Considering those aspects above, the contributions of this paper are summarized as follows. First, the interleave-grid multiple access (IGMA) scheme is evaluated in this paper. The IGMA jointly utilizes the bit-level interleaving and symbol-level sparse grid mapping for simultaneously supporting the sufficient number of multiple access signatures and the reduced detection complexity due to signaling sparsity. Along with iterative detection and decoding receiver, IGMA can provide compelling overloading gain (user multiplexing capability) and achieve very reliable transmission. Meanwhile, IGMA can also leverage the application in mMTC and/or URLLC scenario. Second, evaluation results including link-level simulation (LLS) and system-level simulation (SLS), conducted based on 3GPP 5G new radio (NR) evaluation assumptions and metrics [20], can show the advantages of IGMA, and accordingly IGMA is being considered as a 5G NoMA alternative candidate. Third, to verify the feasibility of IGMA under realistic channel environment, a test bed with up to 12 user equipment (UEs) is also implemented. The results obtained from hardware test bed doubly prove the superiority of IGMA over conventional orthogonal multiple access schemes.

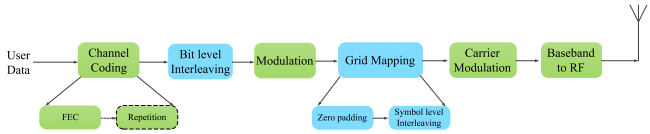

Fig. 1. Schematic example of IGMA transmitter.

The rest of this paper is organized as follows. The transmission and receiving schemes of the proposed IGMA are introduced in Sections II and III, respectively. In Sections IV and V, the evaluation results, including LLS and SLS, are demonstrated to show the performance gain of the proposed IGMA. Section VI introduces the test-bed implementation of IGMA. Finally, conclusions are drawn in Section VII.

II. IGMA Transmission Schemes

We proposed the original idea of IGMA as a class of novel NoMA transmission techniques in [21] and [22]. As shown in Fig. 1, an IGMA multiple user case is considered. The kth user data sequence is denoted as $\mathbf{d}_k$, the coded bit sequence $\mathbf{b}_k$ is obtained by the channel coding process, i.e., $\mathbf{b}_k = [\mathbf{b}_k(1)\ \mathbf{b}_k(2) \ldots\ \mathbf{b}_k(M)]^T$, where M is the length of $\mathbf{b}_k$ and $(\cdot)^T$ denotes the transpose operation. Here, the channel coding process could either apply low rate forward error correction (FEC) code directly or a combination of a moderate rate FEC code and repetition code to achieve low coding rate. When the repetition code is used, there is a tradeoff between sacrificing a certain level of coding gain and reducing the processing complexity.

A. Interleaving Process

For a bit-level interleaver represented by θ_{k-b}, the coded bit sequence $\mathbf{b}_k$ is permuted, where length of θ_{k-b} is equal to length of $\mathbf{b}_k$. The interleaving process is based on a permutation matrix $\boldsymbol{\alpha}_I$, e.g., as shown in (1) when $M = 4$, θ_{k-b}, $\boldsymbol{\alpha}_I$ could be

$$\theta_{k-b} = \{4, 2, 3, 1\} \rightarrow \alpha_I = \begin{bmatrix} 0 & 0 & 0 & 1 \\ 0 & 1 & 0 & 0 \\ 0 & 0 & 1 & 0 \\ 1 & 0 & 0 & 0 \end{bmatrix} \tag{1}$$

where the position of "1" element in the θ_{k-b} indicates each row of permutation matrix $\boldsymbol{\alpha}_I$. Thus, the bit sequence through interleaving process is $\mathbf{c}_k = \boldsymbol{\alpha}_I \cdot \mathbf{b}_k$.

Note that the bit-level interleaver in IGMA schemes is one dimension for user multiplexing. In other words, the IGMA system can separate different UEs based on the UE-specific bit-level interleaver only. In the practical scenario, the scrambling process that has similar functionality could be considered to replace the interleaving process. After bit-level interleaving, the

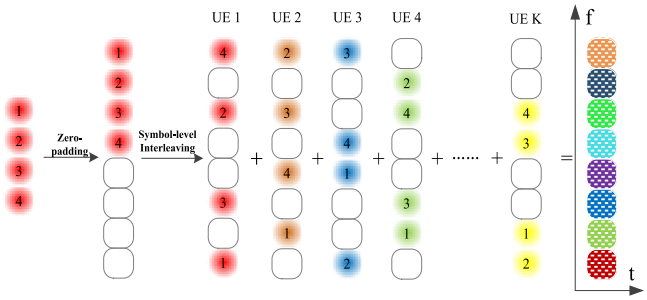

Fig. 2. Grid-mapping example with $N = 4$, $\rho_k = 0.5$, and $L = 8$.

interleaved bit sequence is passed through modulation module to generate symbol sequence.

B. Grid-Mapping Process

In grid-mapping process, the modulated symbol sequence $\mathbf{s}_k = [\mathbf{s}_k(1)\ \mathbf{s}_k(2) \ldots\ \mathbf{s}_k(N)]^T$ is first processed according to different grid-mapping patterns, and processes targets to map the modulated symbols into the allocated resource elements (REs) sparsely. In general, further symbol-level interleaving or symbol-level scrambling could be considered to pursue further interference randomization. Thus, symbol-level interleaving processor θ_{k-s} and zero padding processor are used to execute the grid-mapping process.

In the grid-mapping pattern, a density ρ_k is defined as $\rho_k = N_{\text{used}}/N_{\text{all}}$, where N_{used} is the actually occupied RE number, and N_{all} is the overall assigned RE number. Various level of diversity order can be adopted by choosing different value of ρ_k. After the grid-mapping pattern, the obtained symbol sequence is denoted as $\mathbf{x}_k = [\mathbf{x}_k(1)\ \mathbf{x}_k(2) \ldots\ \mathbf{x}_k(L)]^T$. Thus, the number of "0" elements in $\mathbf{x}_k$ is (L–N). Taking a grid-mapping process example of $N = 4$, $\rho_k = 0.5$, and $L = 8$, the symbol-level processor θ_{k-s}, the density ρ_k, and a permutation matrix $\boldsymbol{\alpha}_{\text{GM}}$ are formulated as

$$\begin{cases} \theta_{k-s} = \{4,0,2,0,0,3,0,1\} \\ \rho_k = 0.5 \end{cases} \rightarrow \boldsymbol{\alpha}_{\text{GM}} = \begin{bmatrix} 0 & 0 & 0 & 1 \\ 0 & 0 & 0 & 0 \\ 0 & 1 & 0 & 0 \\ 0 & 0 & 0 & 0 \\ 0 & 0 & 0 & 0 \\ 0 & 0 & 1 & 0 \\ 0 & 0 & 0 & 0 \\ 1 & 0 & 0 & 0 \end{bmatrix}. \tag{2}$$

As shown in Fig. 2, the zero value denotes the corresponding "0" row of the permutation matrix $\boldsymbol{\alpha}_{\text{GM}}$, and the nonzero value in θ_{k-s} represents the position of "1" element in the corresponding row of permutation matrix $\boldsymbol{\alpha}_{\text{GM}}$. Furthermore, the $\mathbf{x}_k$ is obtained by $\boldsymbol{\alpha}_{\text{GM}} \cdot \mathbf{s}_k = [\mathbf{s}_k(4)0\ \mathbf{s}_k(2)0\ 0\ \mathbf{s}_k(3)0\ \mathbf{s}_k(1)]^T$.

It is worth noting that it is still preferred to configure with identical density at the same resources for the purpose of user multiplexing, even though the density is different by meeting different UEs various requirements. The reason behind is that the complexity from joint detection and decoding in practical scenario, and a regular sparse mapping is beneficial even with mathematic proof [23].

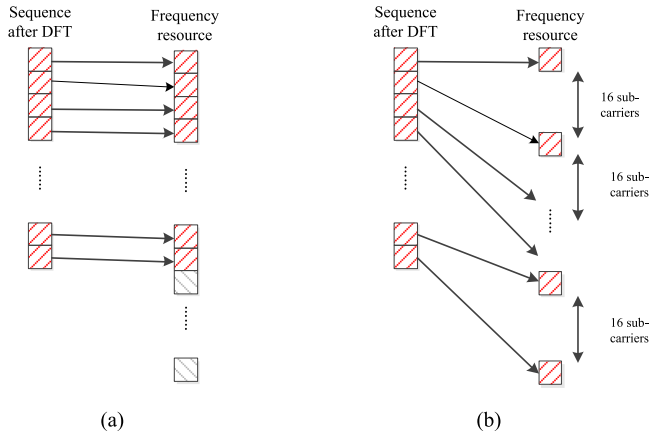

Fig. 3. Two subcarrier mapping ways.

By utilizing symbol-level interleaving process, the symbol sequence order after the grid-mapping process is randomized. This randomness supports to obtain further benefits on combating multipath fading and intercell interference (ICI). In addition, the grid-mapping pattern is also capable for providing another dimension for usermultiplexing. Thus, the IGMA system could either make the user-specific grid-mapping pattern only (or bit-level interleaver only), or it can separate users based on the bit-level interleaver and grid-mapping pattern simultaneously.

It is worth noting that the grid-mapping process can achieve another advantage with proper operations of IGMA. That is, the ICI can be further reduced by fully utilizing the sparse feature of grid mapping for the purpose of coordination among different base stations. Taking an example with two adjacent base stations, if two groups of nearly orthogonal grid-mapping patterns choosing, the number of overlapped symbols among all signals is reduced, leading to the ICI being obviously alleviated. In the simulation part, simulation results will prove the benefits for ICI cancelation.

C. Low Peak-to-Average Power Ratio (PAPR) Consideration

During the standardization discussion of 5G, it has already agreed that orthogonal frequency-division multiplexing (OFDM) is mostly used for the uplink transmission. However, severer PAPR will result in UE suffering from nonlinear distortion when passing through high power amplifier. Hence, discrete Fourier transform (DFT) spreading OFDM (DFT-s-OFDM) with lower PAPR is adopted in the 4G Long Term Evolution (LTE) system. Thus, using DFT-s-OFDM will be an attractive solution for the mMTC UE.

Fig. 3 shows two ways of subcarrier mapping for combining IGMA with DFT-s-OFDM. In Fig. 3(a), localized subcarrier mapping is utilized, which means that continuous subcarriers are selected for one or a group of UEs. Meanwhile, in Fig. 3(b), distributed subcarrier mapping is considered. For each UE or

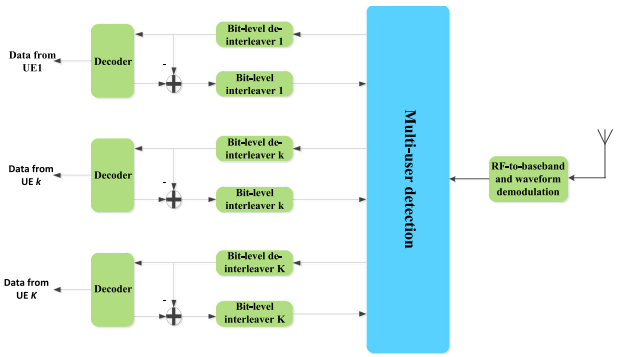

Fig. 4. Schematic example of IGMA receiver.

UE group, subcarriers with equal distance are chosen for data transmission. According to the property of DFT and inverse DFT (IDFT), if distributed subcarrier mapping way in Fig. 3(b) is deployed, and the IDFT size is integer times of DFT size, then the output of IDFT is repetition of input of DFT. As a result, the PAPR of DFT-s-OFDM-based IGMA is only determined by modulation level and the density of grid mapping. Note that for IGMA combining with DFT-s-OFDM, subcarrier mapping can be also regarded as one way to distinguish UEs.

Assuming for the kth UE, the sequence vector after grid-mapping operation is denoted as $\mathbf{v}_k$ with length L; the transmitted symbol vector $\mathbf{x}_k$ with length L_N is calculated as

$$\mathbf{x}_k = \mathbf{W}_{L_N}^{-1}\mathbf{P}\mathbf{W}_L\mathbf{v}_k \tag{3}$$

where $\mathbf{W}_L \in C^{L\times L}$ denotes L-point DFT matrix and its element on the nth row and mth column is $\exp\{-j2\pi\frac{mn}{L}\}$. $\mathbf{W}_L^{-1}$ denotes L-point IDFT matrix and $\mathbf{P} \in C^{L_N\times L}$ denotes a permutation matrix representing subcarrier mapping operation. Specifically, if the mth element after DFT is mapped to the nth subcarrier, then the elements on the nth row and mth column of $\mathbf{P}$ is 1, otherwise 0.

III. IGMA Receiving Schemes

In this section, we first develop and compare different kinds of detection algorithms for IGMA as making balanced tradeoff between computational complexity and system performance. The receiver diagram of IGMA is shown in Fig. 4. To improve the detection performance, the iterative detection and decoding structure is applied. The received signal passes through RF-to-baseband and waveform demodulation module, and is inputted to multiuser detector. The multiuser detector processes the received signal with the *a priori* information of data for each UE from previous iterations, and outputs the *extrinsic* information of data for each UE. Note that to simplify the calculation, soft information, which is presented by log-likelihood ratio (LLR), is utilized in the iteration procedure. For binary information, LLR for bit b is calculated as

$$\mathrm{LLR}(b) = \ln\frac{P(b=+1)}{P(b=-1)}. \tag{4}$$

For the kth UE, the output LLR_k^d of multiuser detector passes through bit-level deinterleaver and decoder. The *a posteriori* probability decoder is applied. The *extrinsic* information LLR_k^c of UE k after the decoder is generated according to the *a posteriori* information from decoder and the input of decoder. LLR_k^c passes through bit-level interleaver and is used as *a priori* information LLR_k^a for the next iteration. Note that considering there is no *a priori* information for the first iteration, we assume $\mathrm{LLR}_k^a = 0$. The iteration between detection and decoding exchanges the *extrinsic* information and reliability is improved after each iteration. The iteration is stopped if the predefined maximum iteration number is reached and the hard decision is used as the estimated data for UE k.

For such a receiver structure depicted in Fig. 4, the receiver complexity mainly comes from detector. For the benefits of using bit-level interleaver, which decorrelates the adjacent coded bits, and grid-mapping procedure, which provides symbol-level density, the detection complexity of IGMA can be significantly reduced. Here, two detection algorithms for IGMA are introduced, namely elementary symbol estimator (ESE) and chip-by-chip MAP detector. While the former is to achieve the tradeoff between detection complexity and detection performance, the latter one holds the preference to obtain better detection and decoding performance.

A. Elementary Symbol Estimator for IGMA

For simplicity of illustration, BPSK is assumed to be used in this section. Actually, it is easy to extend the ESE detection algorithm to higher order modulation schemes, for example, QPSK. The OFDM is utilized as the scheme of carrier modulation and carrier demodulation has been performed, which means that single-tap frequency-domain channel coefficient is considered.

When the IIoT application employing IGMA with shared time–frequency resources, the UEs data bits transmit over multiple access channels, and the received signal $r(m)$ is the summation of all users' signals plus the additive white Gaussian noise $e(m)$

$$r(m) = \sum_{k=1}^{K} h_k x_k(m) + e(m),\ m = 1, 2, \ldots, M \tag{5}$$

where h_k denotes the kth user's frequency-domain channel coefficient and m denotes the bit index. Focusing on the kth UE's data $x_k(m)$, the IGMA receiver will consider others' signals as MUI. Thus

$$r(m) = h_k x_k(m) + \delta_k(m) \tag{6}$$

where $\delta_k(m)$ denotes the overall interference plus noise as

$$\delta_k(m) = \sum_{k'\neq k, k'\in\mathbf{G}_k(m)} h_{k'}x_{k'}(m) + e(m) \tag{7}$$

where $\mathbf{G}_k(m)$ denotes the set contains all the UEs superposed on the mth chip according to the grid-mapping pattern.

By recalling from the central limit theorem, $\delta_k(m)$ could be approximated as a Gaussian variable, and the mean $E(\delta_k(m))$

and variance $\mathrm{Var}(\delta_k(m))$ are given as

$$E\left(\delta_k\left(m\right)\right) = E\left(r\left(m\right)\right) - h_k E\left(x_k\left(m\right)\right) \tag{8}$$

$$\mathrm{Var}\left(\delta_k\left(m\right)\right) = \mathrm{Var}\left(r\left(m\right)\right) - |h_k|^2 \mathrm{Var}\left(x_k\left(m\right)\right). \tag{9}$$

Furthermore, based on (8) and (9), the conditional probability density function of $r(m)$ is obtained by

$$p\left(r\left(m\right)|x_k\left(m\right)=\pm 1\right) = \frac{1}{\sqrt{2\pi \mathrm{Var}\left(\delta_k\left(m\right)\right)}} \times \exp\left(-\frac{\left(r\left(m\right)-\left(\pm h_k + E\left(\delta_k\left(m\right)\right)\right)\right)^2}{2\mathrm{Var}\left(\delta_k\left(m\right)\right)}\right). \tag{10}$$

Based on (10), the extrinsic LLR for UE *k* can be calculated.

According to the central limit theorem approximation, more UEs will make the approximation even more accurate in the case of multiuser multiplexing. This is reasonable in the IIoT applications in which massive connected sensors/devices coexist in the same environment.

From the above-mentioned derivation, we can observe that by utilizing central limit theorem (CLT) approximation, the complexity of multiuser detector is reduced significantly. From the performance perspective, ESE is very suitable for low coding rate schemes. However, for high coding rate schemes, the performance degradation is large, since the coding gain is less such that it cannot compensate the performance loss caused by MUI.

B. Chip-by-Chip MAP Detector

Considering for IGMA, bit-level interleaving can reduce the correlation between adjacent coded bits, which facilitate chip-by-chip detection. Meanwhile, grid-mapping procedure makes that the number of UEs superposed at the same symbol is limited, which can reduce the detection complexity. All above factors make it possible for IGMA to use chip-by-chip MAP detector.

The probability density function of $r(m)$ conditioned on the $b_k(m)$ is calculated as

$$p\left(r\left(m\right)|b_k\left(m\right)=b\right) = \frac{1}{\sqrt{2\pi\sigma^2}} \sum_{\{x(m),b_k(m)=b\}} \times \exp\left(-\frac{\left[r\left(m\right)-\sum_{i=1}^{K} h_i x_i\left(m\right)\right]^2}{2\sigma^2}\right) \tag{11}$$

where the summation condition $\{x(m), b_k(m)=b\}$ denotes all the possible combinations of $\{\mathbf{x}_i(\mathrm{m}), i=0,\ldots,K-1\}$ with $b_k(m)=b$, taking the grid-mapping pattern into considerations.

For IGMA, the LLR for the *k*th UE is calculated as

$$\mathrm{LLR}_k^d\left(m\right) = \ln\frac{p\left(r\left(m\right)|b_k\left(m\right)=+1\right)}{p\left(r\left(m\right)|b_k\left(m\right)=-1\right)}. \tag{12}$$

By using max-log-MAP approximation, the computational complexity of (12) can be further reduced.

C. Modified ESE for Low PAPR IGMA

For DFT-s-OFDM-based IGMA proposed in Section II, the chip-by-chip MAP detector will introduce much higher complexity, due to the property of DFT-s-OFDM. Meanwhile, the ESE introduced in Section III should be modified. Specifically, joint Gaussian distribution is utilized, and the matrixwise operations are applied to replace the elementwise operations in (5)–(10).

D. Complexity Analysis

In this section, we analyzed the complexity of the proposed detection algorithms based on real-valued flops, which can be denoted as a real-valued multiplication or addition.

For specific matrices $\mathbf{A}\in\mathbb{C}^{m\times n}$, $\mathbf{B}\in\mathbb{C}^{n\times p}$, $\mathbf{C}\in\mathbb{C}^{n\times 1}$, and $\mathbf{D}\in\mathbb{C}^{n\times 1}$, the operations of $\mathbf{AB}$, $\|\mathbf{C}\|_F^2$, and $\mathbf{C}\pm\mathbf{D}$ require $8mnp-2\mathrm{mp}$, $4n-1$, and $2n$ flops, respectively.

Accordingly, the complexity of the IDMA-MAP detector C_{MAP} and the modified IDMA-ESE detector C_{ESE} can be computed by

$$C_{\mathrm{MAP}} = 13\,NKN_rM^K + TN\left\{(1+K)M^K + 2KM^K + K\right\} \tag{13}$$

and

$$C_{\mathrm{ESE}} = KN_r\left(24KN + 46N + 16N\right). \tag{14}$$

The details of the complexity of the IDMA-MAP detector C_{MAP} and the modified IDMA-ESE detector C_{ESE} are given as follows. First, the complexity of the IDMA-MAP detector C_{MAP} is mainly invoked by (11). In (11), $13NKN_rM^K$ flops are desired.

1) The calculation of the message from the user node to the source node is $TN(1+K)M^K$.
2) The calculation of the posterior probability of each user is $2TNKM^K$.
3) The calculation of the extrinsic information of each user is TNK.

The complexity of the modified IDMA-ESE detector C_{ESE} is mainly invoked by the following three aspects.

1) The calculation of the mean of variance of the received signal is $KN_r(24KN)$.
2) The calculation of the mean of variance of the interference signal is $KN_r(46N)$.
3) The calculation of the ESE estimator is $KN_r(16N)$.

In general, the complexities C_{MAP} and C_{ESE} are simplified to the order of magnitudes as

$$C_{\mathrm{MAP}} = O(NKM^K),\ C_{\mathrm{ESE}} = O\left(NK^2N_r\right). \tag{15}$$

IV. Link-Level Evaluation Results

In this section, simulation results have been conducted to verify the gains of IGMA. Here, the results of link-level evaluation are presented in this section. First, the evaluation assumptions are listed in Table I. Note that the SNR is defined as per UE transmitted SNR.

In Fig. 5, the evaluation results by using ESE detector with 120-b transport block size (TBS) are demonstrated. As can be observed, the differences between the performances for variable supported number of UEs are negligible; for the case of 6 UEs, 8 UEs, and 10 UEs, the block error rate (BLER) performances

TABLE I
LLS EVALUATION PARAMETERS

Parameters	Values or assumptions
Carrier Frequency	2 GHz
Waveform	OFDM
Channel coding	LTE Turbo
Numerology	15 kHz sub-carrier spacing
System Bandwidth	10 MHz
Total allocated bandwidth	6RBs (1.08Mhz), considering DMRS overhead, 144 available RE per RB
TB size & supported UE number	***ESE detector:*** ✧ 6 RBs (without CRC) :{ 62, 84, 120, 148, 165, 192, 228, 264, 300} (bits); ✧ Supported UE numbers: {6, 8, 10, 12} (equivalent overloading factor: {150%, 200%, 250%, 300%}) ***Chip-by-Chip MAP case:*** ✧ 6 RBs (without CRC) :{84, 120, 192, 264, 408, 624 } (bits); ✧ Supported UE numbers: {6, 12} (equivalent overloading factor: {150%, 300%})
BS antenna config.	2Rx
UE antenna config.	1Tx
Channel estimation	Perfect Realistic
SNR distribution	Equal average SNR
Propagation channel model	TDL-A TDL-C 3km/h in [25]
Detection method	ESE detector, Chip-by-Chip MAP

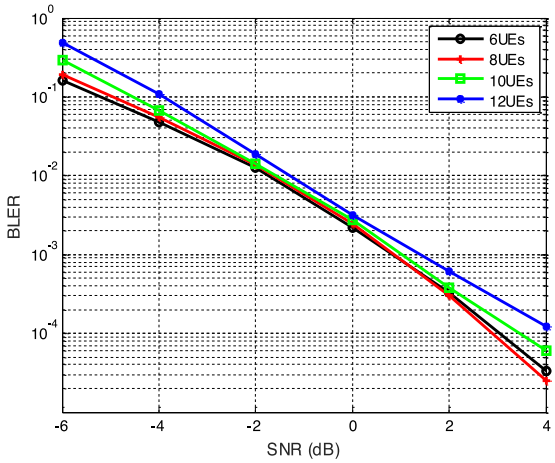

Fig. 5. Grid-mapping example with $N = 4$, $\rho_k = 0.5$, and $L = 8$.

are nearly the same. Even for 12 UEs case, only some trivial the performance degradation is observed. For BLER $= 10^{-2}$, the performance difference is less than 0.5 dB. Note that 120-b TBS will result in using a low coding rate, which is suitable for ESE detector. For higher coding rate, the detection performance will be degraded.

Fig. 6 shows the sum-throughput evaluation results. The sum throughput is calculated for BLER $= 0.1$. As shown in the figure, with low coding rate (low sum-throughput region), increasing the number of supported UEs will directly increase

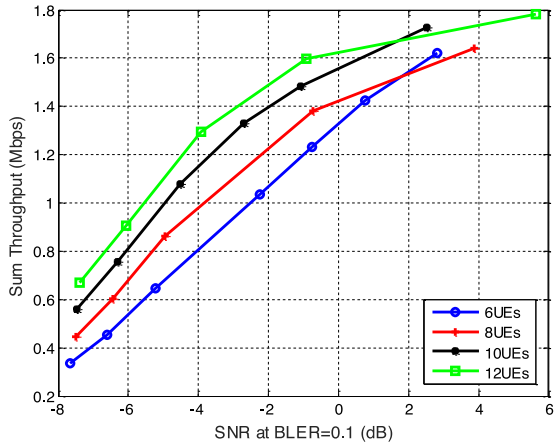

Fig. 6. Sum-throughput evaluation for ESE detector.

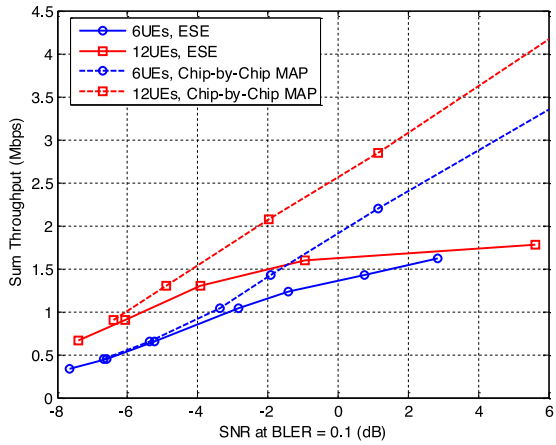

Fig. 7. Sum-throughput evaluation for chip-by-chip MAP detector.

the achievable sum throughput. For example, at SNR $= -2$ dB, compared with 6 UEs case, the sum throughputs are increased by 15%, 33%, and 42%, if the supported UE number is increased to 8, 10, and 12, respectively. However, for high coding rate (high sum-throughput region), the enhancement on sum throughput is not as large as that for low coding rate. This is caused by the fact that ESE detection algorithm is very effective for low coding rate scenarios, but not suitable for high coding rate scenarios [11].

In Fig. 7, the sum-throughput evaluation results by utilizing chip-by-chip MAP detector are illustrated. The detection performance is improved with chip-by-chip MAP detector, especially for high coding rate. From Fig. 7, we can observe that even for high sum-throughput region, the performance improvement due to increasing the number of UEs is still significant. Compared with 6 UEs case with ESE detector, the sum throughputs are increased by 60% and 100% for 6 UEs case and 12 UEs case with chip-by-chip MAP detector, respectively. Considering that by using grid mapping with sparsity, the detection complexity is reduced and the tradeoff between complexity and performance can be achieved.

The performance of IGMA with realistic channel estimation is also evaluated and the corresponding results are shown in Fig. 8. Two types of demodulation reference signal (DMRS)

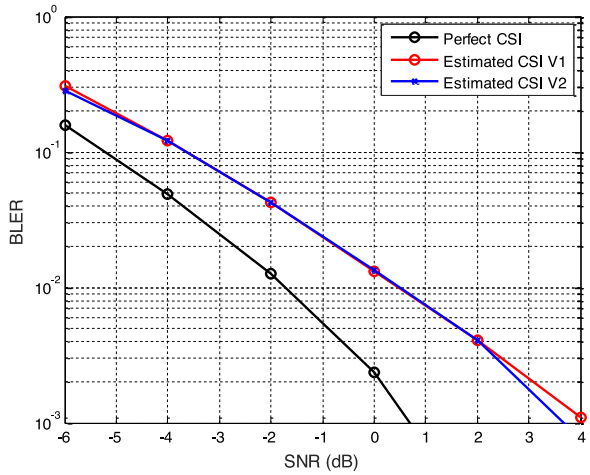

Fig. 8. Performance comparison between perfect and real channel estimation.

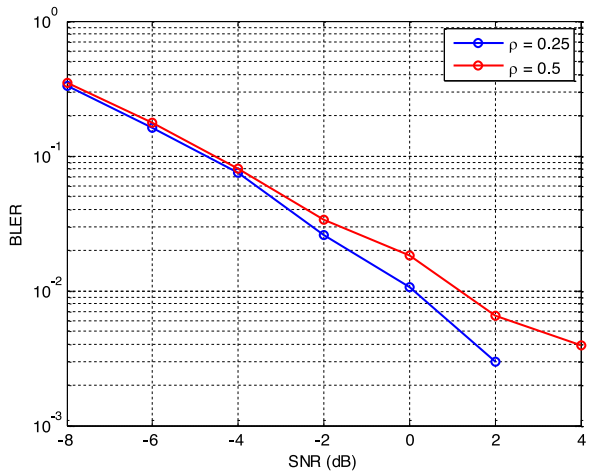

Fig. 9. Performance evaluation with 1 ICI-UE.

are considered. Specifically, the first-type DMRS (V1) denotes using the combination of cyclic shift based on the same root sequence and orthogonal cover code, whereas the second-type DMRS (V2) denotes using the combination of orthogonal cover code, comblike structure, and cyclic shift. The MMSE channel estimation with linear interpolation is applied in the simulation. As can be observed in Fig. 8, the performance loss caused by realistic channel estimation is acceptable. There is about 1.5 dB loss for BLER $= 10^{-1}$. Note that the different types of DMRS have negligible influence on performance.

For multicell scenario, ICI caused by UEs in the neighboring cell will degrade the performance of UEs in the targeting cell. For NoMA scheme, ICI will become more serious since a larger number of UEs occupy the same time/frequency resources. However, due to the sparsity of grid mapping, IGMA can provide ability of combating ICI. Here, we also evaluate the performance of IGMA under multicell scenario.

Figs. 9 and 10 show the evaluation results of IGMA under multicell scenario, with 1 ICI-UE and 2 ICI-UEs, respectively. In the evaluation, the densities of grid-mapping pattern are set as $\rho = 0.5$ and $\rho = 0.25$. TBS is fixed as 120 b and the number

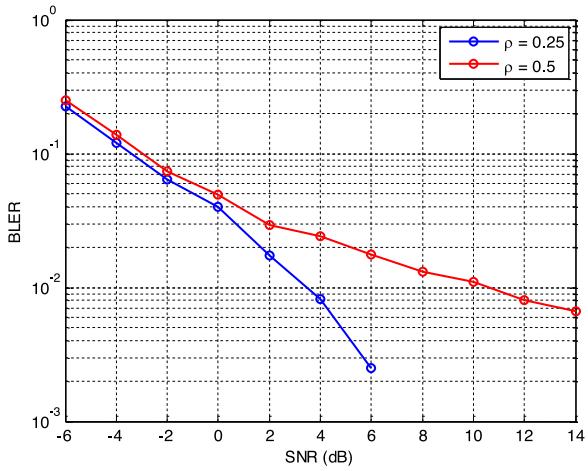

Fig. 10. Performance evaluation with 2 ICI-UE.

of UEs in target cell is set to 6. From the evaluation results, we can observe that by reducing the density of grid-mapping pattern, the performance of IGMA is also improved, especially for the case with 2 ICI-UE. For example, for BLER $= 10^{-2}$, the performance is improved by more than 6 dB if the density is reduced from 0.5 to 0.25. Note that with the coordination between adjacent base stations, the effect of ICI can be further reduced since quasi-orthogonal grid-mapping patterns, or even orthogonal grid-mapping patterns can be selected by these base stations.

Above evaluation results show that the proposed IGMA scheme has the ability of supporting much more UEs, and combating ICI in multicell scenario. Following demonstration will show that with the same evaluation assumption, IGMA will outperform the conventional OFDMA scheme. To ensure fair comparison, the number of supported UEs and transport block (TB) size are set to the same. Specifically, the number of UEs is 6 and the TB size is 120 b. For OFDMA, each UE occupies one physical resource block (PRB) in a distributed way so that frequency diversity gain can be obtained as well. Here, two modulation coding scheme (MCSs) are considered for OFMDA, e.g., QPSK with 1/2 coding rate and 16 quadratic-amplitude modulation with 1/4 coding rate.

The evaluation results are shown in Fig. 11. Note that the SNR definition is different from above figures. Specifically, SNR in Fig. 11 is defined as total received SNR. From Fig. 11, it is obvious that with the same spectral efficiency, IGMA outperforms conventional OFDMA scheme in terms of reliability. At BLER $= 10^{-2}$, the performance gain of IGMA is about 1–2 dB, for different MCSs. It should be noted that if larger TB size or larger number of UEs is considered, the performance gain of IGMA will be larger, since the equivalent coding rate of OFDMA is higher.

V. System-Level Evaluation Results

In this section, the system-level evaluation for IGMA is introduced to show the performance gain over conventional OFDM schemes. For SLS, the performance metric of packet drop rate (PDR) is considered for a given packet arrival rate (PAR). The

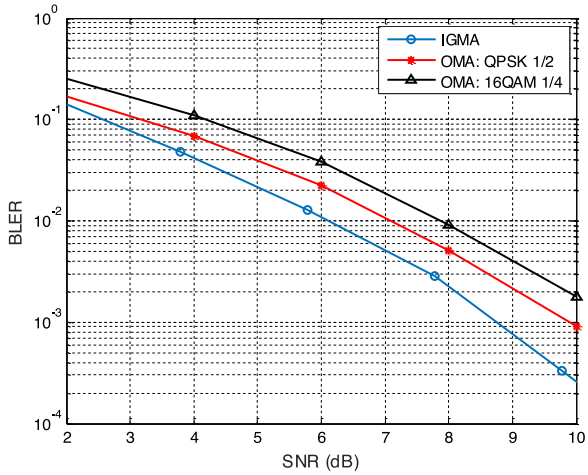

Fig. 11. Performance comparison between IGMA and OFDMA.

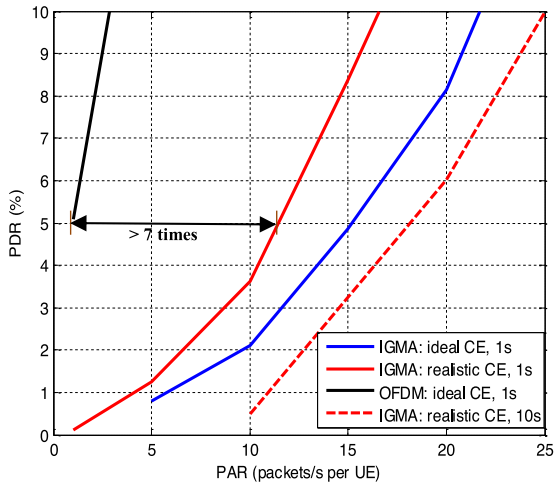

Fig. 12. SLS evaluation results of IGMA.

TABLE II
SLS EVALUATION ASSUMPTIONS

Parameters	Values or assumptions
Layout	Single layer - Macro layer: Hex. Grid
Inter-BS distance	1732 m
Carrier frequency	700 MHz
Simulation bandwidth	6 PRBs
Channel model	3D UMa
Tx power	UE: Max 23 dBm
BS antenna configuration	Rx: 2 ports
BS antenna pattern	Follow the modeling of [25]
BS antenna height	25 m
BS antenna tilt	102° according to the definition in TR36.873
BS antenna element gain + connector loss	8 dBi, including 3dB cable loss
BS receiver noise figure	5 dB
UE antenna elements	1 Tx
UE antenna height	Follow the modeling of [26]
UE antenna gain	-4 dBi
Traffic model	Modified FTP model 3. Packet size is fixed as 20 bytes.
UE distribution	20% of users are outdoors (3km/h) 80% of users are indoor (3km/h) Users dropped uniformly in entire cell
BS receiver	Chip-by-chip MAP detector
UL power control	Open loop power control $\alpha = 1, P_0 = -90$ dBm
Channel estimation	Ideal/realistic

evaluation assumptions are listed in Table II. The number of UEs is set as fixed as 20 per sector.

Note that to enhance the reliability, the HARQ retransmission is employed. To simplify the evaluation, we assume that all the UEs are under radio resource control (RRC)-connected mode and base station can combine each retransmission for each UE. In the evaluation, dropping timer is defined as maximum transmission duration for one package. One package will continue retransmissions until the successful reception or reaching the dropping timer. Two dropping timers are defined, i.e., 1 and 10 s. Besides, the duration between two retransmissions for the same package is set to eight transmission time intervals.

In Fig. 12, the SLS evaluation results are shown. It is clear that, even with realistic channel estimation, IGMA scheme achieves significant gains over OFDM schemes. Under the assumption of 1-s dropping timer, compared with LTE OFDM scheme with ideal channel estimation, for 5% PDR, IGMA can provide more than seven times higher PAR, even with realistic channel estimation. For 10-s dropping timer, the performance improvement for IGMA is even larger, since the reliability of data transmission is better. This result indicates that IGMA can provide capability to support much more UEs compared with existing OFDM.

In the SLS, the number of UEs is fixed to simplify the evaluation. Considering that the interference level for small number of UEs with large PAR is nearly the same with large number of UEs with small PAR, we can deduce the connection density with the assumption of PAR of mMTC scenario. Assume the PAR of mMTC scenario is λ_{mMTC}, the number of UEs set for SLS evaluation is N_{UE} per sector, and the maximal PAR obtained by SLS evaluation for given PDR threshold $p_{\mathrm{SLS}}\%$ is λ_{SLS}; then, the connection density for mMTC scenario is calculated as

$$\rho_{m\mathrm{MTC}} = \frac{N_{\mathrm{UE}}\lambda_{m\mathrm{MTC}}}{\lambda_{\mathrm{SLS}}} \frac{1}{S_{\mathrm{sector}}} \tag{16}$$

where S_{sector} denotes the area of each sector.

Assume PAR per UE for mMTC scenario is 2 h and 8 min (7680 s), which is the same with the assumption for narrowband Internet of Things. According to Fig. 12, the maximal PAR and 1-s dropping timer is 5.82 packets/s per UE for 1% PDR threshold with realistic channel estimation. Based on above evaluation results, the connection density for IGMA assuming six PRBs is calculated as

$$\rho_{\mathrm{IGMA,\ 1s}} = \frac{20{*}7680{*}5.82}{S_{\mathrm{Sector}}} = 1.03{*}10^6\ \mathrm{per\,km}^2. \tag{17}$$

While for 10-s dropping timer, the maximal PAR is about 11 packets/s per UE, and the connection density assuming six

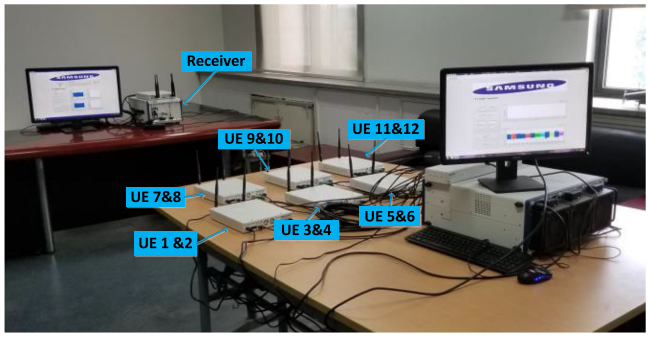

Fig. 13. Test bed for IGMA verification.

TABLE III
EVALUATION ASSUMPTIONS FOR IGMA TEST BED

Parameters	Values
FFT size	2048
CP overhead	1/8
Sample rate ($1/T_s$)	0.5 MHz
Symbol duration	(1+1/8)*1024*T_s =2.304ms
Bandwidth	500 kHz
Number of RBs	72
Sub-carrier spacing	0.49 kHz
Number of occupied sub-carriers	864
TBS	120 bits (CRC not included)
Maximum delay spread	2.51us
Number of data symbol per frame	14 (including two DMRS symbols)
Detection algorithm	Chip-by-chip MAP

PRBs and 1% PDR is computed as follows:

$$\rho_{\mathrm{IGMA}_{,10s}} = \frac{20*7680*11}{S_{\mathrm{Sector}}} = 1.95*10^6 \,\mathrm{per\,km^2}. \quad (18)$$

From (17) and (18), we can observe that even with realistic channel estimation and 1-s dropping timer, the one million per km^2 connection density requirements for mMTC scenario can be fulfilled by IGMA. Note that six PRBs are assumed in evaluation. If larger bandwidth is allowed, larger connection density can be achieved.

The above evaluation demonstrates that the proposed IGMA scheme has the potential to satisfy the requirements on connection density of NR mMTC scenario.

VI. TEST-BED IMPLEMENTATION OF IGMA

In this paper, we also set up one test bed by using National Instrument software defined platform to verify the feasibility of IGMA under realistic channel environment. As shown in Fig. 13, 12 UEs with single antenna are considered. Meanwhile, two received antennas are equipped at receiver. The distance between UEs and receiver is 35 cm. The evaluation assumptions are listed in Table III.

The evaluation results obtained from test bed are illustrated in Fig. 14. Both 6 UE case and 12 UE case are evaluated. To

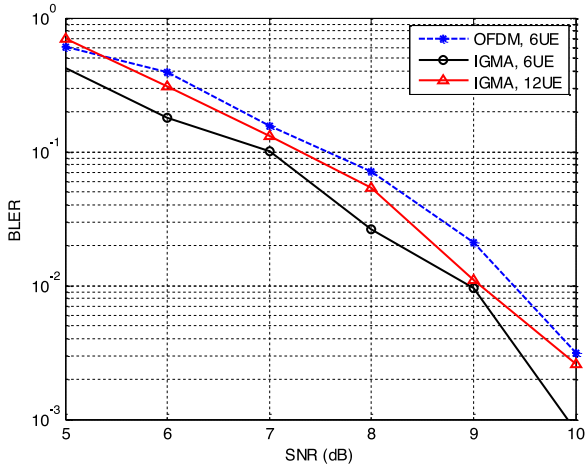

Fig. 14. Evaluation results for IGMA test bed.

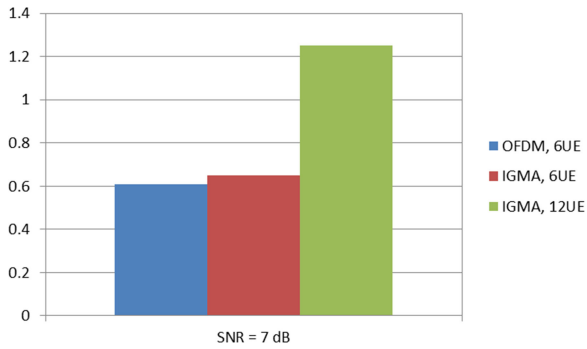

Fig. 15. Sum data rates comparison in kbits for three transmit schemes.

verify the performance gain of IGMA, OFDMA with 6 UEs is also evaluated under the same configurations. To get a fair comparison results, the data rates for IGMA and OFDMA are set to be the same. Note that for OFDM, 144 subcarriers are occupied by each UE. From Fig. 14, it can be observed that with the same number of UEs, IGMA outperforms OFDMA. For example, for BLER $= 10^{-1}$, the performance gain over OFDMA is more than 0.5 dB. Even with doubled number of UEs, IGMA still outperforms OFDM. At BLER $= 10^{-1}$, IGMA with 12 UEs has about 0.2 dB performance gain compared with OFDM with 6 UEs. This result is aligned with LLS evaluation results, which indicates the validity of test-bed evaluation results.

To further illustrate the gain of IGMA, the sum data rate is also obtained from test bed and the corresponding results are shown in Fig. 13. The SNR is selected as 7 dB since the BLERs are around 10^{-1}. The BLER is considered during the sum data rate calculation. From Fig. 13, we can observe that by increasing the number of UEs, IGMA can improve the sum data rate significantly compared with OFDM in terms of overall received data rates. In the case shown in Fig. 15, the system data rate is improved more than two times.

Fig. 16 compares the complexity of the IDMA-MAP detector C_{MAP} and the modified IDMA-ESE detector C_{ESE} for the QPSK-aided IGMA systems with $N = 864$, $N_r = 2$, and 6

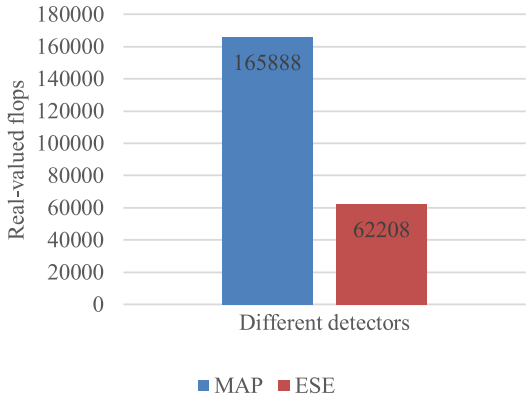

Fig. 16. Complexity comparison of the IGMA-MAP detector and the modified IGMA-ESE detector.

UEs. As shown in Fig. 16, the modified IDMA-ESE detector can achieve 62% complexity reduction over the IDMA-MAP detector.

VII. Conclusion

IIoT is a network consisted of multiple devices. Compared with cellular communication system, the number of devices is usually much larger, with relatively low data rates. Meanwhile, the low cost devices are more preferable in IIoT scenario and the reliability is also a key metric, especially for factory scenarios. In this paper, we have proposed an alternative NoMA scheme, namely as IGMA. Typically, IGMA can provide high adaptability toward massive connections, and efficiently support higher capacity and robustness with greater flexibility by utilizing the interleaving and grid-mapping process. Hence, IGMA is very suitable for IIoT scenario, since the number of supported devices can be increased. Considering low coding rate is used, reliability can be also guaranteed. Sparsity introduced by symbol-level grid mapping provides robustness to interference, especially ICI. Evaluation results, including LLS and SLS, show that IGMA can achieve significant performance gain in terms of BLER, sum throughput, and supportable connection density in a limited bandwidth compared with LTE OFDMA, e.g., as much as seven times in terms of supported UE number. Furthermore, a hardware test bed verified the practical feasibility of the proposed IGMA and proved the advantage of IGMA, e.g., as twice sum data rate as that of LTE OFDMA. Conclusively, the developed IGMA was motivated by industry interest of new 5G usage scenarios and turns out to be a strong enabler for 5G business thriving, with great practical potentials and implementability.

References

[1] A. Orsino *et al.*, "Effects of heterogeneous mobility on D2D- and drone-assisted mission-critical MTC in 5G," *IEEE Commun. Mag.*, vol. 55, no. 2, pp. 79–87, Feb. 2017.

[2] Y. Sun *et al.*, "Optimal resource allocation for NOMA-TDMA scheme with α-fairness in industrial internet of things," *Sensors*, vol. 18, no. 5, p. 1572, 2018, https://doi.org/10.3390/s18051572.

[3] Y. Han, Z. Wang, D. Li, Q. Guo, and G. Liu, "Low-complexity iterative detection algorithm for massive data communication in IIoT," *IEEE Access*, vol. 6, pp. 11166–11172, 2018.

[4] T. Kim, I. Kim, Y. Sun, and Z. Jin, "Physical layer and medium access control design in energy efficient sensor networks: An overview," *IEEE Trans. Ind. Inform.*, vol. 11, no. 1, pp. 2–15, Feb. 2015.

[5] A. J. Viterbi, "Very low rate convolutional codes for maximum theoretical performance of spread spectrum-multiple-access channels," *IEEE J. Sel. Areas Commun.*, vol. 8, no. 4, pp. 641–649, May 1990.

[6] H. Kim, Y. G. Lim, C. B. Chae, and D. Hong, "Multiple access for 5G new radio: Categorization, evaluation, and challenges," 2017. [Online]. Available: https://arxiv.org/pdf/1703.09042.pdf

[7] F. N. Brannstrom, T. M. Aulin, and L. K. Rasmussen, "Iterative detectors for trellis-code multiple-access," *IEEE Trans. Commun.*, vol. 50, no. 9, pp. 1478–1485, Sep. 2002.

[8] P. Frenger, P. Orten, and T. Ottosson, "Code-spread CDMA with interference cancellation," *IEEE J. Sel. Areas Commun.*, vol. 17, no. 12, pp. 2090–2095, Dec. 1999.

[9] R. H. Mahadevappa and J. G. Proakis, "Mitigating multiple access interference and intersymbol interference in uncoded CDMA systems with chip-level interleaving," *IEEE Trans. Wireless Commun.*, vol. 1, no. 4, pp. 781–792, Oct. 2002.

[10] J. Y. Zhu, J. H. Wang, Y. M. Huang, S. W. He, X. H. You, and L. Yang, "On optimal power allocation for downlink non-orthogonal multiple access systems," *IEEE J. Sel. Areas Commun.*, vol. 35, no. 12, pp. 2744–2757, Dec. 2017.

[11] Q. H. Du, H. B. Song, and X. J. Zhu, "Social-feature enabled communications among devices towards smart IoT community," *IEEE Commun. Mag.*, to be published.

[12] Z. Li, B. Chang, S. Wang, A. Liu, F. Zeng, and G. Luo, "Dynamic compressive wide-band spectrum sensing based on channel energy reconstruction in cognitive internet of things," *IEEE Trans. Ind. Inform.*, vol. 14, no. 6, pp. 2598–2607, Jun. 2018.

[13] L. Ping, L. Liu, K. Y. Wu, and W. K. Leung, "On interleave-division multiple-access," in *Proc. IEEE Int. Conf. Commun.*, Paris, France, 2004, pp. 2869–2873.

[14] L. Ping, L. Liu, K. Wu, and W. K. Leung, "Interleave division multiple access," *IEEE Trans. Wireless Commun.*, vol. 5, no. 4, pp. 938–947, Apr. 2006.

[15] Study on Non-Orthogonal Multiple Access for NR, 3GPP TSG RAN Meeting #75, Sophia Antipolis Cedex, France, RP-170383, pp. 1–5, 2017.

[16] H. Nikopour and H. Baligh, "Sparse code multiple access," in *Proc. Int. Symp. Pers., Indoor, Mobile Radio Commun.*, 2013, pp. 332–336.

[17] X. Dai *et al.*, "Successive interference cancelation amenable multiple access (SAMA) for future wireless communications," in *Proc. IEEE Int. Conf. Commun. Syst.*, 2014, pp. 222–226.

[18] V. D. Beek and B. M. Popovic, "Multiple access with low-density signatures," in *Proc. IEEE Global Telecommun. Conf.*, 2009, pp. 1–6.

[19] M. Zhao, S. Zhou, W. Zhou, and J. Zhu, "An improved uplink sparse coded multiple access," *IEEE Commun. Lett.*, vol. 21, no. 1, pp. 176–179, Jan. 2017.

[20] Z. Yuan, G. Yu, W. Li, Y. Yuan, X. Wang, and J. Xu, "Multi-user shared access for internet of things," in *Proc. IEEE Veh. Technol. Conf.*, 2016, pp. 1–5.

[21] 3GPP TSG RAN WG1, R1-1612569 DFT-based IGMA scheme, Samsung, Nov. 2016.

[22] 3GPP TSG RAN WG1, R1-1612575 Considerations on evaluation method for IGMA, Samsung, Nov. 2016.

[23] Study on New Radio (NR) Access Technology; Physical Layer Aspects, 3GPP TR 38.802, Release 14, 2017.

[24] O. Shental, B. M. Zaidel, and S. S. Shitz, "Low-density code-domain NoMA: Better be regular," in *Proc. IEEE Int. Symp. Inf. Theory*, 2017, pp. 2628–2632.

[25] Study on Channel Model for Frequency Spectrum Above 6 GHz, 3GPP TR 38.900, Release 14, 2016.

[26] Study on 3D Channel Model for LTE, 3GPP TR 36.873, Release 12, 2015.

[27] Q. Xiong, C. Qian, B. Yu, and C. Sun, "Advanced NoMA scheme for 5G cellular network: Interleave-grid multiple access," in *Proc. IEEE Global Telecommun. Conf. Workshops*, 2017, pp. 1–5.

Su Hu received the M.S. and Ph.D. degrees from the National Key Laboratory on Communications, University of Electronic Science and Technology of China (UESTC), Chengdu, China, in 2007 and 2010, respectively.

From 2011 to 2012, he was a Research Fellow with the School of Electrical and Electronic Engineering, Nanyang Technological University, Singapore. He is currently a Full Professor with the UESTC. His research interests include sequence design with good correlation properties and physical layer design for wireless communication system, such as filter bank multicarrier systems and cognitive radio networks.

Bin Yu received the M.S. degree in electrical engineering from the University of Southampton, Southampton, U.K., in 2006.

He is currently a Director of Communication Research Laboratory, Beijing Samsung Telecom R&D Center of Samsung Electronics, Beijing, China, leading 5G R&D and standardization. He has more than ten years of experience in mobile communication field and has been working on various standards, including TD-SCDMA, HSPA+, LTE, and LTE-A since July 2006. His research interests include advanced waveform, nonorthogonal multiple access, flexible duplexing, artificial intelligent assisted wireless, etc.

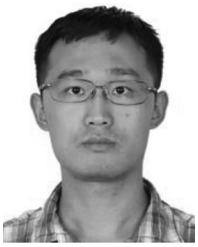

Chen Qian received the Ph.D. degree in electrical engineering from Tsinghua University, Beijing, China, in 2015.

In 2015, he joined the Communication Research Laboratory, Beijing Samsung Telecommunication R&D Center, Beijing, China, as a 5G Research Engineer. His research interests include MIMO system, waveform design, nonorthogonal multiple access, 5G communication PHY/MAC design, etc. He is currently involved in standardization for 5G in 3GPP.

Yue Xiao was born in Jiangsu, China, in 1979. He received the Ph.D. degree in electrical engineering from the School of Communications and Information Engineering, University of Electronic Science and Technology of China, Chengdu, China, in 2007.

His research interests include wireless communications, including beyond 5G communication systems, spread spectrum systems, and digital signal processing.

Qi Xiong received the Ph.D. degree in electrical and electronic engineering from Nanyang Technological University, Singapore, in 2015.

In 2015, he joined the Communication Research Laboratory, Beijing Samsung Telecommunication R&D Center, Beijing, China, as a 5G Research Engineer. His research interests include physical layer security, nonorthogonal multiple access, 5G communication PHY/MAC design, etc. He is currently involved in standardization for 5G in 3GPP.

Chengjun Sun received the Doctorate degree in signal and information processing from the Harbin Institute of Technology, Harbin, China, in 2003.

He is currently a Senior Director and Head of the Standard and Research Team, Beijing Samsung Telecom R&D Center, Beijing, China, responsible for standard and research of mobile communication technologies. In 2003, he started working with the Samsung Electronics in standard and research work of TD-SCDMA and WCDMA with the main focus on physical layer key technology research and performance requirements. Then, he led the 3GPP standard activities and strategy in Samsung China including RAN1, RAN3, and RAN4 standardization. Since 2015, he has been leading the overall standard and research activities in Samsung China, which cover next generation cellular technology research, 3GPP standardization, and China domestic standardization.

Yuan Gao (M'14) received the B.S. degree from PLA Information Engineering University, Zhengzhou, China, in 2008, and the M.S. and Ph.D. degrees from the Department of Electronic Engineering, Tsinghua University, Beijing, China, in 2011 and 2014, respectively, all in electrical engineering.

He is currently an Assistant Professor with Tsinghua University and China Defense Science and Technology Information Center. He has authored or coauthored more than 40 academic papers in peer-reviewed international journals and conferences. His research interests include wireless communication system, satellite communication system, network control theory, and big data.

Prof. Gao is a member of ACM. He is an Associate Editor for several international journals, including the IEEE ACCESS, *EURASIP Journal on Wireless Communications and Networking*, *Sensors*, etc. He is also a Guest Editor of several special issues. He is also a Guest Reviewer and TPC Member for several journals and international conferences, including the IEEE JOURNAL ON SELECTED AREAS IN COMMUNICATIONS, the IEEE TRANSACTIONS ON WIRELESS COMMUNICATION, the IEEE TRANSACTIONS ON COMMUNICATION, the IEEE COMMUNICATION LETTER, ICC, WCNC, etc.